A Fast Beam-Ion Instability

G. V. Stupakov

Stanford Linear Accelerator Center, Stanford University, P.O. Box 4349, Stanford, CA 94309

Abstract

The ionization of residual gas by an electron beam in an accelerator generates ions that can resonantly couple to the beam through a wave propagating in the beam-ion system. Results of the study of a beam-ion instability [1,2] are presented for a multi-bunch train taking into account the decoherence of ion oscillations due to the ion frequency spread and spatial variation of the ion frequency. It is shown that the combination of both effects can substantially reduce the growth rate of the instability.

I. INTRODUCTION

A fast beam-ion instability which is caused by the interaction of a single electron bunch train with the residual gas ions, has been studied recently in Ref. [1,2]. The instability mechanism is the same in both linacs and storage rings assuming that the ions are not trapped from turn-to-turn. The ions generated by the head of the bunch train oscillate in the transverse direction and resonantly interact with the betatron oscillations of the subsequent bunches, causing the growth of the initial perturbation of the beam.

The nature of the instability closely resembles the beam-breakup instability due to transverse wakefields. It differes from instabilities previously studied [3-9], where the ions, usually treated as being in equilibrium, interact with a circular electron or proton beam. The instability we discuss can occur in a transport line, linac, or a storage ring with a clearing gap to prevent ion trapping.

An important element that has to be included into the treatment of the instability is a frequency spread within the ion population. It is known that the frequency spread and associated with it decoherence in an instability problem usually results in Landau damping effect and in some situations can suppress the instability. We show that although the ion frequency spread does not fully suppress the instability, it decreases the growth rate making it in a typical situations two or tree times smaller than that predicted without decoherence effects.

We also consider spatial modulation of the ion frequency due to the variation of the beta and dispersion functions along the beam path. It turns out that combination of this variation with the frequency spread can substantially weaken the instability. This is not a very important effect in a FODO lattice, but it could prove to be much more significant in other lattices such as the TBA or Chasman-Green structures used in many synchrotron light sources.

For the sake of simplicity, we focus on the interaction of an electron beam with ions, although similar effects apply to a positron beam trapping free electrons.

The variation of the ion frequency ω_i included in this paper is caused by two sources. One of them is due to the horizontal beam density profile in a flat beam which causes the local ion frequency to depend on the horizontal position. Another source of spread in ω_i is the nonlinearity of the ion oscillations inside the beam.

For analytical study we adopt a model that treats the bunch train as a continuous beam. This model is applicable if the distance between the bunches l_b is smaller than the betatron wavelength, $l_b \ll c/\omega_\beta$ and the ion oscillation wavelength $l_b \ll c/\omega_i$. This condition is well satisfied for multi-bunch machines such as the PEP-II High Energy Ring [11] or the NLC Damping Ring [12]. We assume a one-dimensional model that treats only vertical linear oscillation of the centroids of the beam and the ions.

The paper is structured as follows. In Section II, the differential equations of motion are derived. Section III discusses averaging of the equations based on different time scales associated with oscillations and growth of the instability. The ion frequency spread and

resulting decoherence of ion oscillations are analyzed in Section IV. Analytical and numerical solutions of the equations for the NLC Damping Ring and PEP-II High Energy Ring are presented in Sections V and VI respectively. They are compared with direct computer simulation of the instability in Section VII. Effects of spatial ion frequency variation are discussed in Sections VIII and IX. The results are summarized in Section X.

II. THE EQUATIONS OF MOTION

We will assume a rigid vertical motion of the beam and define the offset of the centroid at time t and longitudinal position s as $y_b(s,t)$. The distance s is measured from the injection point at $t = 0$. The equation for the beam centroid, including the interaction with the ion background, is

$$\left(\frac{1}{c}\frac{\partial}{\partial t} + \frac{\partial}{\partial s}\right)^2 y_b(s,t) + \frac{\omega_\beta^2}{c^2} y_b(s,t) = \kappa \cdot (ct - s)\left(y_i(s,t) - y_b(s,t)\right) . \tag{1}$$

The left hand side of this equation accounts for the free betatron oscillation of a moving beam (we assume $v_{beam} \approx c$). On the right hand side, we included the force acting on the beam from the ions whose centroid is offset by $y_i(s,t)$. In the linear theory, this force is proportional to both the relative displacement between the beam and ions centroids and the ion density. Assuming a continuous electron beam with a uniform density per unit length, the ion density increases due to collisional ionization as $ct - s$ (it is equal to zero before the beam head arrives at the point s at time $t = s/c$). After separating the factor $ct - s$ on the right hand side of Eq. (1), the coefficient κ is

$$\kappa \equiv \frac{4\dot{\lambda}_{ion} r_e}{3\gamma c \sigma_y (\sigma_x + \sigma_y)} , \tag{2}$$

where γ denotes the relativistic factor for the beam, r_e is the classical electron radius, $\sigma_{x,y}$ denotes the horizontal and vertical rms-beam size respectively, and $\dot{\lambda}_{ion}$ is the number of ions per meter generated by the beam per unit time. Assuming a cross section for collisional ionization of about 2 Mbarns (corresponding to carbon monoxide at 40 GeV), we have

$$\dot{\lambda}_{ion}[\mathrm{m}^{-1}\mathrm{s}^{-1}] \approx 1.8 \cdot 10^{9} n_e[\mathrm{m}^{-1}] p_{gas}[\mathrm{torr}] \ , \tag{3}$$

where n_e is the number of electrons in the beam per meter, and p_{gas} the residual gas pressure in torr.

To find the equation for ions, we will assume that they perform linear oscillations inside the beam with a frequency ω_i. Furthermore, we will allow a continuous spectrum of ω_i given by a distribution function $f(\omega_i)$ normalized so that

$$\int f(\omega_i)\, d\omega_i = 1 \tag{4}$$

(in Sec. VIII we will consider a more general case when f also depends on s). The spread in ω_i at a given position s (and for a given ion species) is caused by several sources; they are discussed in more detail in Sec. IV. The distribution $f(\omega_i)$ is peaked around the frequency $\omega_i = \omega_{i0}$ corresponding to small vertical oscillations on the axis,

$$\omega_{i0} \equiv \left[\frac{4 n_e r_p c^2}{3A\sigma_y(\sigma_x + \sigma_y)}\right]^{1/2} , \tag{5}$$

where A designates the atomic mass number of the ions, n_e the number of electrons in the beam per unit length, and r_p the classical proton radius ($r_p \approx 1.5 \cdot 10^{-16} cm$). Typically, the frequency spread $\Delta\omega_i$ is not large; we assume $\Delta\omega_i \ll \omega_{i0}$.

We also have to distinguish between the ions generated at different times t' because they will have an initial offset equal to the beam coordinate $y_b(s,t')$. Let us denote by $\tilde{y}_i(s,t|t',\omega_i)$ the displacement, at time t and position s, of the ions generated at t' ($t' \le t$) and oscillating with the frequency ω_i. We have an oscillator equation for $\tilde{y}_i$

$$\frac{\partial^2}{\partial t^2}\tilde{y}_i(s,t|t',\omega_i) + \omega_i^2\left[\tilde{y}_i(s,t|t',\omega_i) - y_b(s,t)\right] = 0 \ , \tag{6}$$

with initial condition

$$\tilde{y}_i(s,t'|t',\omega_i) = y_b(s,t') \ , \quad \left.\frac{\partial \tilde{y}_i}{\partial t}\right|_{t=t'} = 0 \ . \tag{7}$$

Finally, averaging displacement of the ions produced at different times t' and having different frequencies ω_i gives the ion centroid $y_i(s,t)$

$$y_i(s,t) = \frac{1}{t-s}\int_s^t dt' \int d\omega_i f(\omega_i)\tilde{y}_i(s,t|t',\omega_i) \ . \tag{8}$$

Equations (1), (6)-(8) constitute a full set of equations governing the development of the instability in the beam-ion interaction.

III. AVERAGING OF THE EQUATIONS

Equation (6) can be easily integrated with the initial conditions (7) yielding

$$\tilde{y}_i(s,t|t',\omega_i) = y_b(s,t) - \int_{t'}^{t} \frac{\partial y_b(s,t'')}{\partial t''} \cos\omega_i(t-t'')\,dt'' \ . \tag{9}$$

Now using Eq. (8), Eq. (1) reduces to an integro-differential equation

$$\left(\frac{1}{c}\frac{\partial}{\partial t} + \frac{\partial}{\partial s}\right)^2 y_b(s,t) + \frac{\omega_\beta^2}{c^2} y_b(s,t) = -\kappa \int_s^t (ct'-s)\frac{\partial y_b(s,t')}{\partial t'} D(t-t')\,dt' \ , \tag{10}$$

where $D(t-t')$ denotes a decoherence function defined as

$$D(t-t') = \int d\omega_i \cos\omega_i(t-t') f(\omega_i) \ . \tag{11}$$

This function represents the oscillation of the centroid of an ensemble of ions with a given frequency distribution $f(\omega_i)$ having an initial unit offset.

Instead of t and s, it is convenient to transform to new independent variables z and s, where $z = ct - s$. The variable z measures the distance from the head of the beam train and for a fixed z the variable s plays a role of time. Denoting

$$y(s,z) \equiv y_b(s, s+z) \ , \tag{12}$$

Eq. (10) takes the form

$$\frac{\partial^2}{\partial s^2} y(s,z) + \frac{\omega_\beta^2}{c^2} y(s,z) = -\kappa \int_0^z z' \frac{\partial y(s,z')}{\partial z'} D(z-z')\,dz' \ . \tag{13}$$

If $D(z) = \cos\omega_i z$ (no frequency spread), Eq. (13) reduces to the equation derived in Ref. 1.

We will assume that the interaction between the beam and the ions is small,

$$c^2\kappa l \ll \omega_{i0}^2,\ \omega_\beta^2\ , \tag{14}$$

where l denotes the length of the bunch train, so that the instability develops on a time scale which is much larger than both the betatron period and the period of ion oscillations. Typically this inequality is easily satisfied. In such a situation, the most unstable solution of Eq. (13) can be represented as a wave propagating in the beam with a slowly varying amplitude and phase,

$$y(s,z) = \mathrm{Re} A(s,z)\, e^{-i\omega_\beta s/c + i\omega_{i0} z/c}\ , \tag{15}$$

where the complex amplitude $A(s,z)$ is a 'slow' function of its variables,

$$\left|\frac{\partial \ln A}{\partial s}\right| \ll \frac{\omega_\beta}{c}\ ,\quad \left|\frac{\partial \ln A}{\partial z}\right| \ll \frac{\omega_{i0}}{c}\ . \tag{16}$$

For a fixed z, the s-dependence of Eq. (15) describes a pure betatron oscillation, while, for a fixed s (that is in the ion frame of rest), the z-dependent part implies oscillations with the frequency ω_{i0}. Hence the wave resonantly couples the ions and the electrons.

Substituting Eq. (15) into Eq. (13) and averaging it over the rapid oscillations with the frequencies ω_{i0} and ω_β, one finds

$$\frac{\partial A(s,z)}{\partial s} = \frac{\kappa\omega_{i0}}{4\omega_\beta}\int_0^z z' A(s,z')\hat{D}(z-z')\,dz'\ , \tag{17}$$

where the function $\hat{D}(z)$ is

$$\hat{D}(z) = \int d\omega_i f(\omega_i)\, e^{i(\omega_i-\omega_{i0})z/c}\ . \tag{18}$$

One of the advantages of the above approach is that it allows a simple scaling of the instability with the vacuum pressure. Indeed, the only place where the pressure p enters Eq. (17) is the parameter κ which is proportional to p (see Eqs. (2) and (3)). By introducing a new variable $s\kappa$ instead of s, we can eliminate κ from the equation. This means that increasing the pressure n times is equivalent to the shrinking the s axis by the same factor. Thus, having solved Eq. (17) for one particular value of pressure, we can use the result for various p by simply rescaling the s variable, $s \propto p^{-1}$.

IV. ION DECOHERENCE

The frequency spread of the ions at a given longitudinal coordinate s stems from several sources. One of them is a variation of the electron density in the beam along the horizontal axis. Since the ion frequency scales as the square root of the electron density, $\omega_i \propto \sqrt{n_e}$, ions located at different coordinates x in a flat beam will have different ω_i. For a Gaussian distribution of electrons in x, $n_e \propto \exp\left(-x^2/2\sigma_x^2\right)$, and we obtain $\omega_i(x) \propto \exp\left(-x^2/4\sigma_x^2\right)$. Hence,

$$\omega_i(x) - \omega_{i0} = \omega_{i0}\left[\exp\left(-x^2/4\sigma_x^2\right) - 1\right], \tag{19}$$

where ω_{i0} is the frequency at $x = 0$.

To find the decoherence function $\hat{D}$, we will utilize a simple one-dimensional model that assumes that the ion frequency of horizontal oscillations is much smaller than the vertical frequency ω_i, and neglects the horizontal ion motion on the time scale of the decoherence. In this model, the ion distribution in x is the same as the electron distribution (because the rate of ionization is proportional to n_e),

$$f_i(x) = \frac{1}{\sqrt{2\pi}\sigma_x}\exp\left(-x^2/2\sigma_x^2\right), \tag{20}$$

and Eq. (18) takes the form

$$\hat{D}(t) = \int_{-\infty}^{\infty} dx f_i(x)\exp\left\{-i\omega_{i0}t\left[1 - \exp\left(-x^2/4\sigma_x^2\right)\right]\right\}. \tag{21}$$

Note that in this model we overestimate the effect of the decoherence. For flat beams, a typical ratio of the horizontal and vertical oscillation frequencies is roughly 3. Thus, the horizontal motion of the ions modulates the vertical oscillation frequency ω_i between ω_{i0} and $\omega_i(x)$ making the average ω_i smaller than $\omega_i(x)$. To fully account for this effect, one has to deal with the two-dimensional ion motion which would make the consideration much more involved.

At this point, we note that Eq. (21) has been defined as the average offset of the ions at a given s. However, the quantity relevant to the electron-ion coupling is the average force

that acts on the electron beam. The force differs from the average displacement because the ion density decreases with x and thus the ion electric field at the beam edges is suppressed relative to that at the bunch center. To account for this effect, we correct $\hat{D}(t)$ by including the electron density n_e in the integrand of Eq. (21)

$$\hat{D}(t) = \text{const} \int_{-\infty}^{\infty} dx f_i(x) n_e(x) \exp\left[-i\omega_{i0} t \left(1 - e^{-x^2/4\sigma_x^2}\right)\right], \tag{22}$$

where the constant in Eq. (22) must be chosen such that $\hat{D}(0) = 1$. This gives

$$\hat{D}(t) = \frac{1}{\sqrt{\pi}\sigma_x} \int_{-\infty}^{\infty} dx \exp\left[-i\omega_{i0} t \left(1 - e^{-x^2/4\sigma_x^2}\right) - x^2/\sigma_x^2\right]. \tag{23}$$

The plots of the real and imaginary parts of this function are shown in Fig. 1. Asymptotically, for large values of $\omega_{i0}t$,

$$\hat{D}(t) \approx (1 + i\alpha\omega_{i0}t)^{-1/2}, \tag{24}$$

where the numerical factor $\alpha = 1/4$.

Another source of ion decoherence is the nonlinearity of the electron potential. It results in a dependence of ω_i on the amplitude of the oscillation and causes an additional spread in the oscillation frequencies ω_i. We have numerically computed the decoherence function due to nonlinearity in a manner similar to the approach of Ref. 13 ; it is also plotted in Fig. 1. One can show that the decoherence due to nonlinearity has the same asymptotes as Eq. (24) with a somewhat smaller α. In what follows, we will use the simple form given by Eq. (24) for $\hat{D}(t)$ in which we put $\alpha = 3/8$ to account for the additional decoherence due to the nonlinearity.

V. ANALYSIS

Let us for a moment ignore the ion decoherence in Eq. (17) and put $\hat{D}(z) \equiv 1$. In this case, the equation can easily be solved analytically. Differentiation with respect to z, reduces Eq. (17) to the differential equation

$$\frac{\partial^2 A(s,z)}{\partial s \partial z} = \frac{\kappa\omega_{i0}}{4\omega_\beta} z A(s,z) \ . \tag{25}$$

For the initial condition $A(0,z) = 1$, the solution is

$$A(s,z) = I_0\left(z\sqrt{\frac{\kappa\omega_{i0}}{2\omega_\beta}s}\right) \ , \tag{26}$$

where I_0 is the zeroth order Bessel function of imaginary argument. This solution was found in Ref. 1 using a different method. For large values of the argument the asymptotic expansion of the Bessel function yields

$$A(s,z) \approx \left(2\pi z\sqrt{\kappa\omega_{i0}s/2\omega_\beta}\right)^{-1/2} \exp\left(z\sqrt{\kappa\omega_{i0}s/2\omega_\beta}\right) \ , \tag{27}$$

which indicates an instability with a characteristic time $\tau \approx 2\omega_\beta/\kappa\omega_{i0}l^2c$, where l is the length of the bunch train. Note that since $A(s,z) \propto \exp\left(z/l\sqrt{s/c\tau}\right)$, the characteristic time τ does not represent an e-folding time, and the instability develops much slower than it would be in the case of normal exponential growth $\propto \exp(s/c\tau)$.

VI. NUMERICAL RESULTS

To study the effect of the decoherence in more realistic cases, we wrote a computer code that numerically integrates Eq. (17) with $\hat{D}(t)$ given by Eq. (24). The two input parameters for the code are the characteristic time $\tau = 2\omega_\beta/\kappa\omega_{i0}l^2c$, and the train length $\omega_{i0}l/c$.

Simulations have been performed for the NLC Damping Ring and the PEP-II HER. In the NLC Damping Ring (see relevant parameters in Ref. [1]), we assumed a residual gas with a vacuum pressure of $p = 10^{-8}$ Torr and an atomic number of A=28. This corresponds to a characteristic time of $\tau = 45$ ns and a bunch length of $\omega_{i0}l/c = 150$. The results are depicted in Fig. 2 for the initial condition $A(0,z) = 1$; for comparison, in Fig. 3, we plot the solution of Eq. (27) for the same parameters but without the decoherence. The plots show the growth of the beam centroid at 10 positions evenly spaced along the bunch train. Comparing Fig. 2 and 3, shows the decoherence slowing down the instability. To characterize the growth rate of the instability, we defined τ_{growth} as an e-folding time for the

last bunch in the train. Since the instability is not exponential, τ_{growth} varies with time. For the time interval 1 $\mu s < t < 2$ μs, we find that $\tau_{growth} \approx 0.5$ μs without decoherence and $\tau_{growth} \approx 1$ μs with ion decoherence; the decoherence decreases the growth rate by a factor of two.

Figures 2 and 3 illustrate the growth of the instability from an initial condition Eq. (15) which is the most unstable perturbation. In reality, the initial noise in the beam will contain different harmonics of which only one or two, having a spatial period $2\pi c/\omega_{i0}$, are very unstable. Assuming that the number of bunches in the train equals N_b and their displacements are uncorrelated with the rms value of δ, a simple statistical argument shows that the amplitude of harmonics in the bunch will be of the order of $\delta/\sqrt{N_b}$. To illustrate the effect of random initial positions, we integrated Eq. (17) including the effect of the ion decoherence with the initial condition corresponding to uncorrelated displacement with $\delta = 1$ for 90 bunches in the NLC Damping Ring. The result is shown in Fig. 4 for $p = 10^{-9}$ and $p = 10^{-8}$ (as noted in Section III, variation of the pressure simply re-scales the horizontal axis in the plot). The figure shows that the development of the instability is somewhat delayed until the amplitude of the unstable mode with an initial value $\delta/\sqrt{90} \approx 0.1$ reaches the value comparable to 1; for $p = 10^{-8}$, this occurs after roughly $5\mu s$. After this point, the growth proceeds at about the same rate as in Fig. 2.

For the PEP-II High Energy Ring, we assumed a vacuum pressure of $p = 10^{-9}$ Torr and A=28. This corresponds to a characteristic time $\tau = 5.5\mu s$ and a bunch length $\omega_{i0} l/c = 220$. The bunch offsets at 10 positions in the train are shown in Fig. 5 as a function of s for the initial condition $A(0, z) = 1$. From this figure, we estimate that the e- folding growth time, on the time interval 200 $\mu s < t < 400$ μs, is roughly $\tau_{growth} \approx 150$ μs. As noted before, this growth time depends on the interval considered.

VII. COMPUTER SIMULATIONS

Direct macro-particle simulations of the instability have been performed [2] using a computer code described in Ref. 1. In the simulations, each of the bunches is represented by 10,000 macro-particles and they interact with the ions which are represented by roughly 50,000 macro-particles. In this manner, the beam and ion distributions evolve self-consistently as the beam is tracked through the magnet lattice.

The results of a simulation for the NLC Damping Ring with a vacuum pressure of $p = 10^{-8}$ Torr are shown in Fig. 6 where we have plotted the oscillation amplitude, normalized by $\sqrt{N_{macro}}/\sigma_y$; this allows for a direct comparison with Fig. 4. Comparing Fig. 6 with Fig. 4 shows a good agreement for the growth rate of the instability during the initial stage ($t < 6\ \mu s$). At later times, the macro-particle simulation exhibits saturation which is presumably due to the nonlinearity of the beam-ion force as the amplitude of the oscillations become comparable to the rms beam size σ_y; this occurs at a value of 100 in the normalized units of the plot.

VIII. EFFECT OF SPATIAL ION FREQUENCY VARIATION

An inhomogeneity of ω_i has different effect on the instability depending on the typical scale λ_i on which the ion frequency varies. If this scale is much smaller than a half of the wavelength λ_{inst} associated with the instability, $\lambda_{inst} = 2\pi/(\omega_\beta + \omega_i)$, (about 15 m for CO ions in the HER of the PEP-II), $\lambda_i \ll \lambda_{inst}$, fluctuations of ω_i can be considered as an effective frequency spread in the ion population which contributes to Landau damping mechanism. In the opposite limit, $\lambda_i \gg \lambda_{inst}$, one has to deal with the problem where the unstable perturbation propagates in a system which characteristics slowly vary is space.

Here we consider only the effect of long-range variation of the ω_i. They result in breaking the synchronism between the ion and electron oscillations and suppression of the resonant interaction between the species. We will show that this effect may result in a substantial

weakening of the instability.

The governing equation (17) remains valid in the case of slow modulation of the ion frequency if one considers the distribution function $f(s,\omega_i)$ and the decoherence function $\hat{D}(s,z)$ as depending on s. Eq. (18) now takes the form

$$\hat{D}(s,z) = \int d\omega_i f(s,\omega_i)\, e^{i(\omega_i-\omega_{i0})z/c}. \tag{28}$$

We further assume that $f(s,\omega_i)$ is such that

$$f(s,\omega_i) = F(\omega_i - \omega_{i0} - \delta\omega_i(s)), \tag{29}$$

where $\delta\omega_i(s) \ll \omega_{i0}$. This means that moving to a new location s shifts the distribution function in ω_i-space as a whole but does not change its form. Putting Eq. (29) into Eq. (28) yields

$$\hat{D}(s,z) = e^{i\delta\omega_i(s)z/c} D_0(z), \tag{30}$$

where

$$D_0(z) = \int d\omega F(\omega)\, e^{i\omega z/c} \tag{31}$$

is the decoherence function in the homogeneous case given by Eq. (24). We see that inhomogeneity effectively modifies the decoherence function.

IX. NUMERICAL RESULTS AND ANALYSIS

Equation (1) has been integrated numerically for the parameters of the HER of the PEP-II assuming the gas pressure $p = 10^{-9}$ torr of CO (A=28), and

$$\delta\omega_{i0}(s) = a\omega_{i0}\sin(2\pi ns/C,) \tag{32}$$

where C is the circumference of the ring and a is the relative variation of the frequency. Fig. 7 shows the result for 10% variation of ω_{i0}, $a = 0.1$, and $n = 1$. Note the exponential growth of the amplitude with an estimated e-folding time $\tau_e = 400\mu s$ (cf. with 150 μs in

the homogeneous case). Fig. 8 shows the result for $a = 0.3$ and $n = 1$, with the e-folding time about 800 μs.

The exponential nature of the instability and the increase of the growth time can be explained in the following way. Inclusion of the ion frequency variation makes the decoherence function Eq. (30) such that it is effectively localized on a scale that is much smaller than the characteristic distance (in z) on which $A(s,z)$ varies. This allows us to neglect the variation of the $z'A(s,z')$ in the integrand of the right hand side of Eq. (17) and put it in front of the integral,

$$\frac{\partial A(s,z)}{\partial s} \approx \frac{\kappa\omega_{i0}}{4\omega_\beta} z A(s,z) \int_0^z \hat{D}(s,z-z')\,dz' \approx \frac{\kappa\omega_{i0}}{4\omega_\beta} z A(s,z) \int_0^\infty \hat{D}(s,z')\,dz'. \tag{33}$$

Furthermore, since the instability is developing on a large time scale, we can average the function $\hat{D}(s,z)$ over s. This gives

$$\frac{\partial A(s,z)}{\partial s} = \frac{1}{\tau_e c} A(s,z), \tag{34}$$

with the exponential solution

$$A(s,z) = A_0(z) \exp(s/c\tau_e), \tag{35}$$

where

$$\tau_e^{-1} = \frac{\kappa\omega_{i0}c}{4\omega_\beta} z \left\langle \int_0^\infty \hat{D}(s,z')\,dz' \right\rangle, \tag{36}$$

and the angular brackets denote averaging over s. Eq. (36) can be rewritten as

$$\tau_e^{-1} = \frac{1}{2\tau}\frac{z}{l} \left\langle \int_0^\infty \hat{D}(s,z')\,\frac{dz'}{l} \right\rangle, \tag{37}$$

where $\tau = 2\omega_\beta/\kappa\omega_{i0}cl^2$ is the characteristic time introduced Section V ($\tau = 5.5\mu s$ for the HER of the PEP-II), and l is the length of the bunch train. Using Eqs. (37), (30) and (24), one finds

$$\tau_e^{-1} = \frac{1}{2\tau}\frac{z}{l}\frac{c}{al\omega_{i0}} \int_0^\infty \frac{d\xi J_0(\xi)}{(1+i\alpha\xi/a)^{1/2}}. \tag{38}$$

Numerical integration for the above examples gives $\tau_e = 350\mu s$ for $a = 0.1$, $z = l$, and $\tau_e = 760\mu s$ for $a = 0.3$, $z = l$, in good agreement with the simulations.

Asymptotically, for $a > 0.3$, the integral in Eq. (38) approaches 1, yielding a simple formula for τ_e,

$$\tau_e \approx 2\tau \frac{l}{z} \frac{al\omega_{i0}}{c}. \tag{39}$$

In order to apply the above analysis to a particular lattice, it is necessary to include many spatial harmonics in Eq. (32). This has not been accomplish yet. To get a rough estimate of the amplitude of the ion frequency variation we plotted in Fig. 9 the ion frequency (CO) in the PEP-II HER as a function of the position in the ring. The plot indicates that one can expect 10-20% variation of ω_i in the ring.

X. DISCUSSION

In this paper, we described a fast beam-ion instability which can develop in a train of bunches with a clearing gap. We have included into consideration the ion frequency variation due to the nonlinearity of the beam-ion force in both the x and y planes. In general, the dependence of ω_i on the horizontal motion is the more important effect and strictly should be described with a two-dimensional treatment of the ion motion. There are other sources of ion frequency spread that we have not considered although they can be included in our formalism in a straightforward manner.

In all cases, the variation of the ion frequency causes Landau damping and slows the instability growth rate. In the two examples that we studied, the growth rate was reduced by roughly a factor of 2. For longer bunch trains, where the factor $\omega_{i0}l/c$ becomes larger, the reduction of the growth rate should be more pronounced. We should also note that we have characterized the instability with an approximate e-folding time τ_{growth}. While this differs from the characteristic time τ that more accurately describes the instability which grows as $\exp(\sqrt{t/\tau})$, it provides a more intuitive estimate of the impact of the instability.

For example in the PEP-II HER, τ_{growth} is roughly 150 μs while $\tau \approx 6$ μs. This growth rate could be decreased further by adding additional clearing gaps in the bunch train [1]. For example, a second gap will increase the instability rise time to roughly $\tau_{growth} \approx 0.6$ ms which is inside the bandwidth of the feedback system.

Our analytical model is confirmed by comparison with a macro-particle computer simulation and shows a good agreement. An important effect which is not included in the model but will also suppress the instability is the tune spread in the electron beam. The tune spread can arise from the beam energy spread and the chromaticity of the optical lattice, the nonlinearity of the lattice, the space charge force due to the ions or the electrons themselves, or the beam-beam collision in a colliding beam storage ring. For example, in the PEP-II High Energy Ring with a beam-beam collision parameter $\xi = 0.03$, the estimated decoherence time for the betatron oscillations is 200 μs and it is comparable with the growth rate of the instability.

We have shown that even slight variation of the ion frequency along the beam path makes the instability truly exponential and, what is more important, further suppresses the growth rate. For synchrotron light sources, where the ion frequency variation is very large, this mechanism can be a strong stabilizing factor for the fast-ion instability.

XI. ACKNOWLEDGMENTS

We would like to thank A. Chao, S. Heifets, T. Raubenheimer and F. Zimmermann for useful discussions. This work was supported by Department of Energy contract DE-AC03-76SF00515.

REFERENCES

[1] T. O. Raubenheimer and F. Zimmermann. "Fast Beam-Ion Instability: I. Linear Theory and Simulations," submitted to *Phys. Rev. E* and SLAC-PUB-95-6740 (1995).

[2] G. V. Supakov, T. O. Raubenheimer, and F. Zimmermann. "Fast Beam-Ion Instability: II. Effect of Ion Decoherence," submitted to *Phys. Rev. E* and SLAC-PUB-95-6805 (1995).

[3] G. Koshkarev and P. Zenkevich, "Resonance of Transverse Coupled Oscillations in Two Circular Beams,", *Part. Accel.*, **3** (1972) 1.

[4] E. Keil and B. Zotter, "Landau Damping of Coupled Electron-Antiproton Oscillations," CERN ISR-TH/71-58 (1971).

[5] L. J. Laslett et al., "Transverse Two-Stream Instability in the Presence of Strong Species-Species and Image Forces," *Nucl. Instr. and Meth.* **A121** (1974) 517.

[6] R. Alves Pires et al., "On the Theory of Coherent Instabilities Due to Coupling Between a Dense Cooled Beam and Charged Particles from the Residual Gas", *Proc. 1989 Part. Accel. Conf.*, Chicago, p.800.

[7] E. Jones et al., " Transverse Instabilities Due to Beam-Trapped Ions and Charged Matter in the CERN Antiproton Accumulator," *Proc. 1985 Part. Accel. Conf.*, Vancouver, p.2218.

[8] A. Poncet, "Ion Trapping and Clearing," *Proc. 1989 CERN Accel. School*, Uppsala, Sweden, CERN 90-04 (1990).

[9] A. Poncet, "Ions and Neutralization," *Frontiers of Particle Beams: Intensity Limitations*, Lecture Notes in Physics: 400 (Springer-Verlag, Berlin, 1990).

[10] D. Sagan and A. Temnykh, "Observations of the Coherent Beam-Ion Interaction in the CESR Storage Ring," *Nucl. Instr. and Meth.*, **A344** (1994) 459.

[11] PEP-II: An Asymmetric B Factory Conceptual Design Report, SLAC-418 (1993).

[12] Parameters for the NLC Damping Ring can be found in: *Proceedings of the 5th Int. Workshop on Next-Generation Linear Colliders*, Stanford, CA, SLAC-436 (1994).

[13] R.E. Meller, et al. "Decoherence of Kicked Beams," SSC-N-360, 1987.

FIGURES

Figure 1. Real (1) and imaginary (2) parts of the function $\hat{D}(t)$ given by Eq. (23), and the asymptotes of Eq. (24) (dashed lines). Curves 3 and 4 shows real and imaginary parts respectively of the decoherence function due to nonlinearity of the ion motion.

Figure 2. Growth of an initial unit offset in the NLC Damping Ring at 10 different points in the train (the line corresponding to the first point is superimposed on the abscissa) with ion decoherence.

Figure 3. Growth of an initial unit offset in the NLC Damping Ring at 10 different points in the train (the line corresponding to the first point is superimposed on the abscissa) without decoherence.

Figure 4. Instability in the NLC Damping Ring with random initial condition and with ion decoherence.

Figure 5. Growth of an initial unit offset in the PEP-II High Energy Ring.

Figure 6. Macro-particle simulation of of the instability in the NLC Damping Ring with a vacuum pressure of 10^{-8} Torr and A=28; the position of every 10th bunch is plotted.

Figure 7. Instability in the PEP-II High Energy Ring for 10% variation of the ion frequency. The vertical scale is logarithmic.

Figure 8. Instability in the PEP-II High Energy Ring for 30% variation of the ion frequency.

Figure 9. The oscillation frequency for CO ions in the PEP-II HER as a function of the position in the ring.

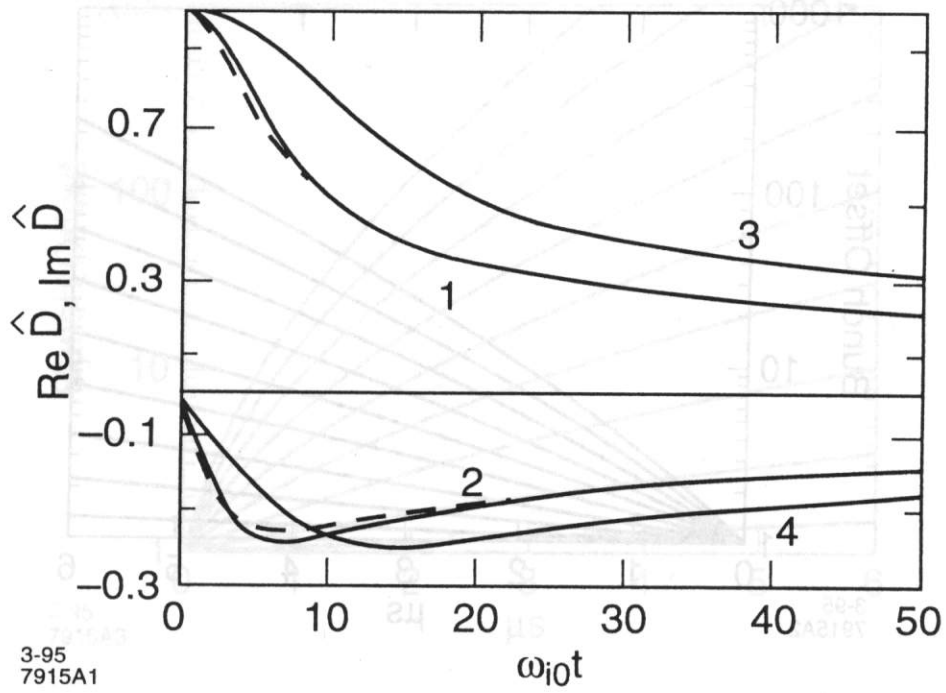
0.7
0.3
−0.1
−0.3
0
10
20
30
40
50
$\omega_{i0}t$
$\mathrm{Re}\,\hat{D}, \mathrm{Im}\,\hat{D}$
1
2
3
4
3-95
7915A1

Fig. 1.

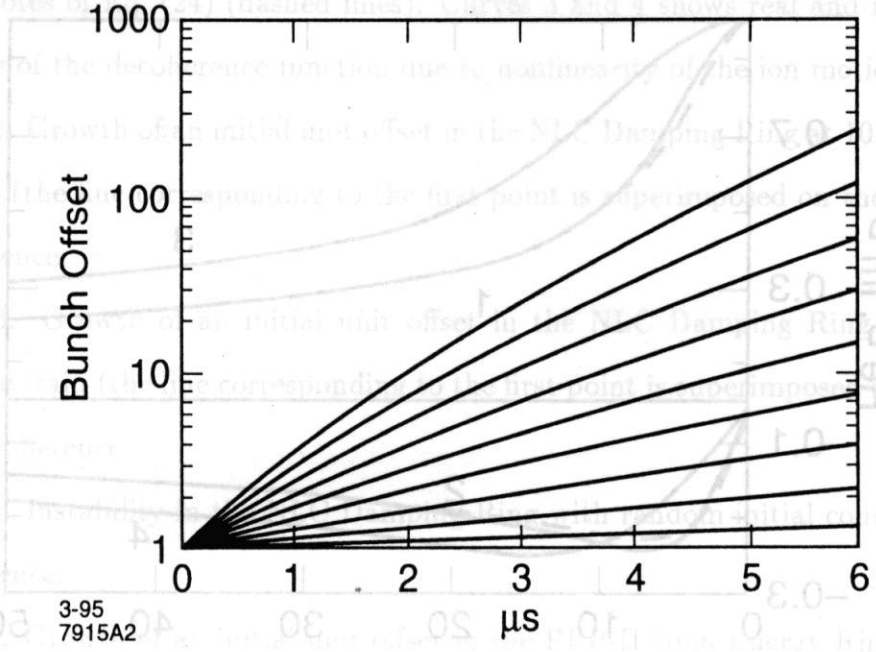

Fig. 2.

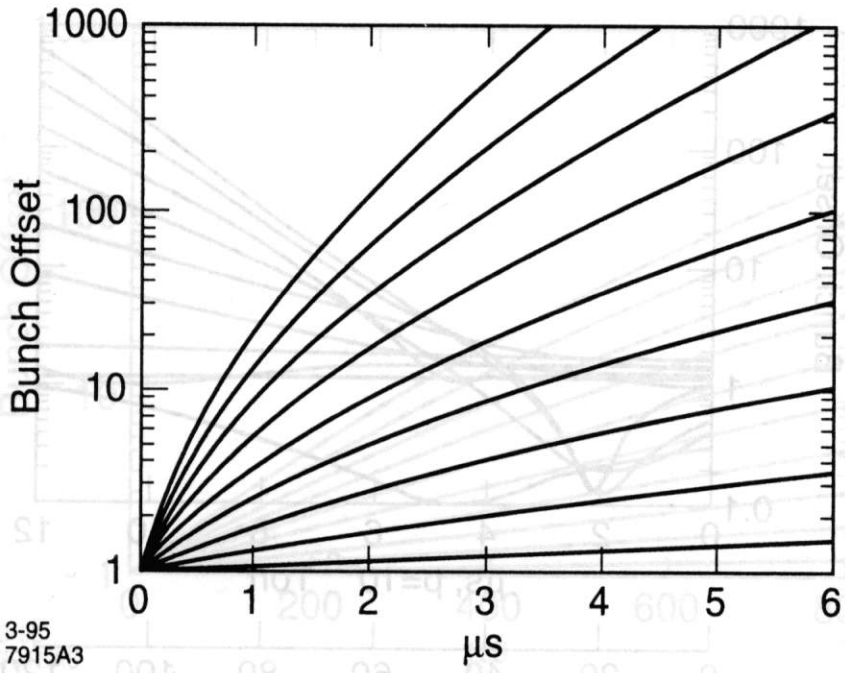

Fig. 3.

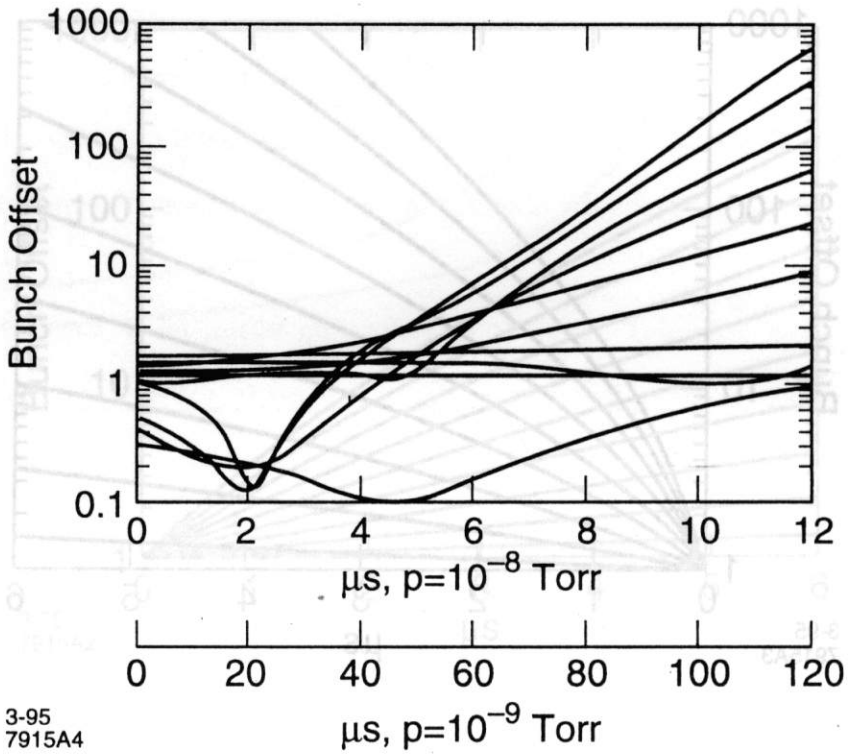
1000
100
10
1
0.1
Bunch Offset
0
2
4
6
8
10
12
μs, p=10^−8 Torr
0
20
40
60
80
100
120
μs, p=10^−9 Torr
3-95
7915A4

Fig. 4.

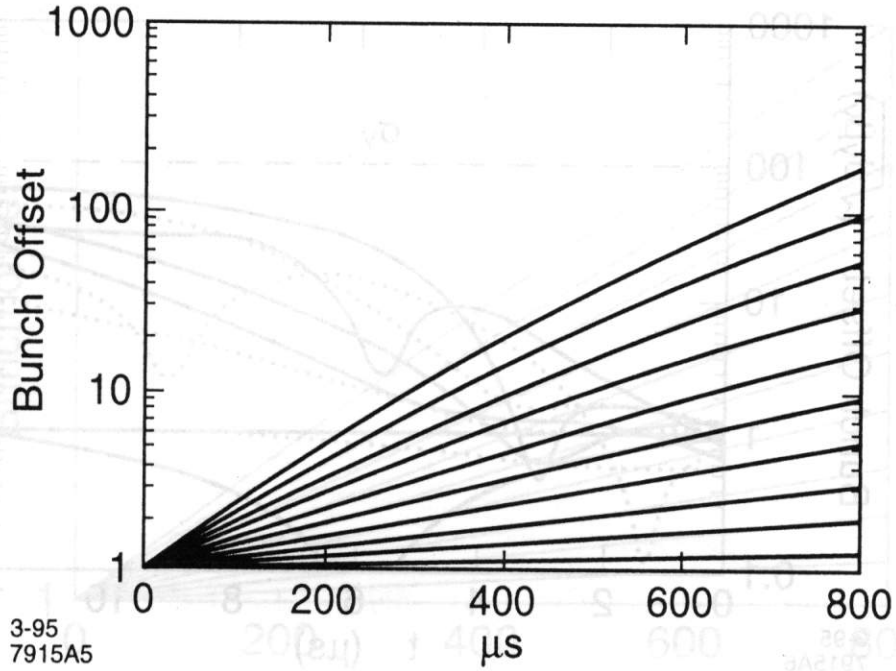

Fig. 5.

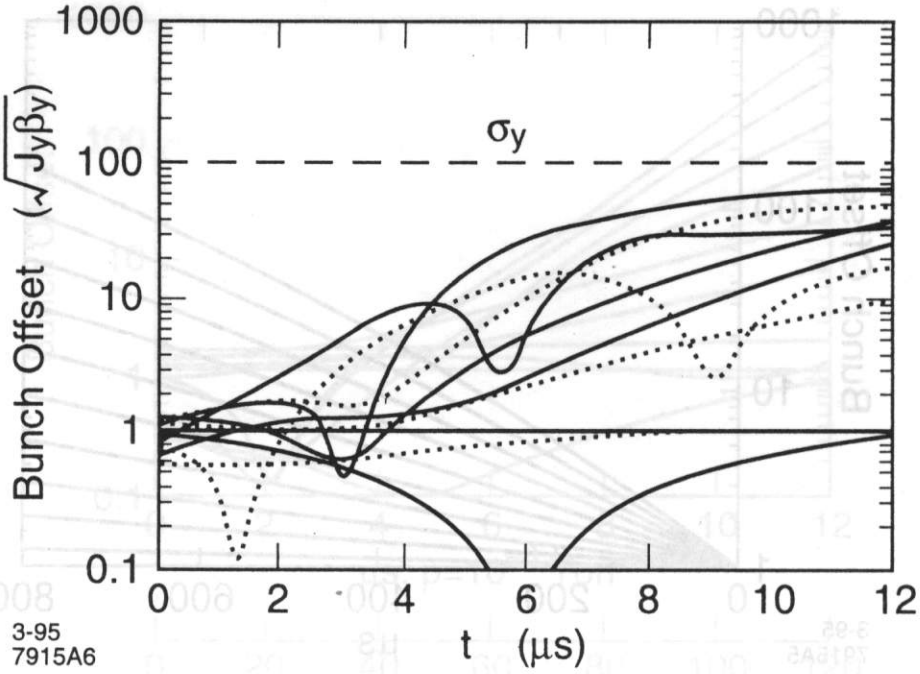
1000
100
10
1
0.1
σ_y
Bunch Offset $(\sqrt{J_y\beta_y})$
0
2
4
6
8
10
12
t (μs)
3-95
7915A6

Fig. 6.

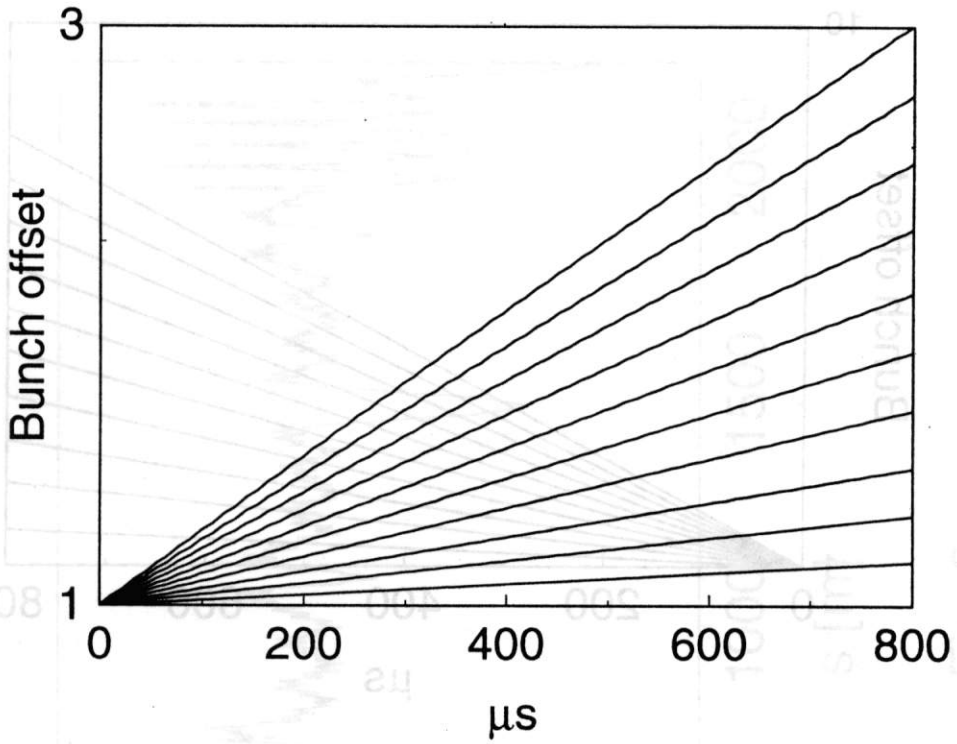

Fig. 7.

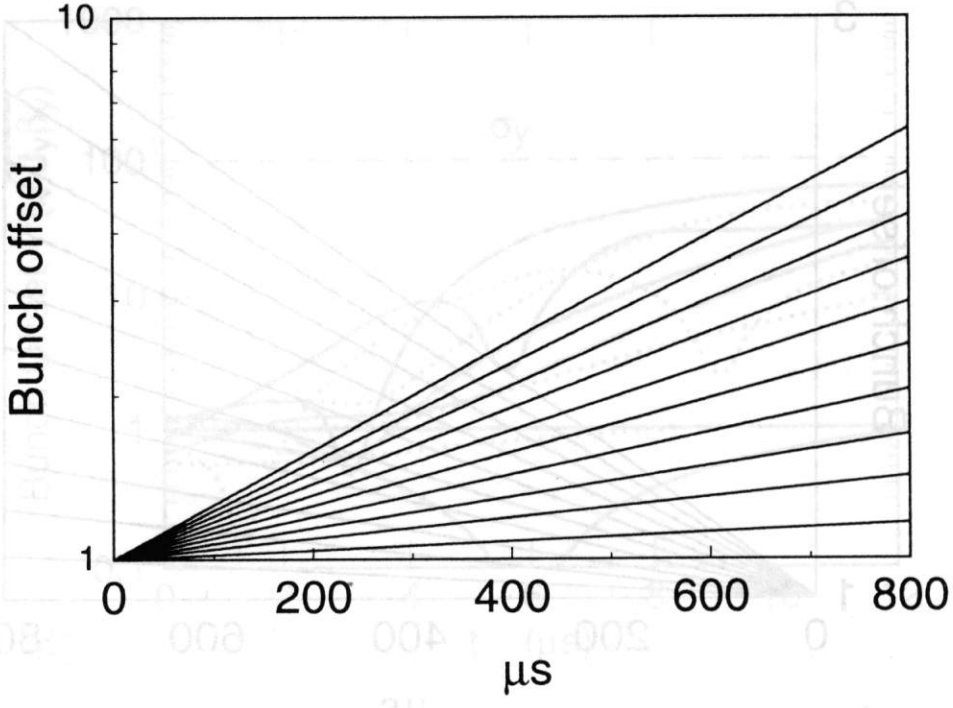

Fig. 8.

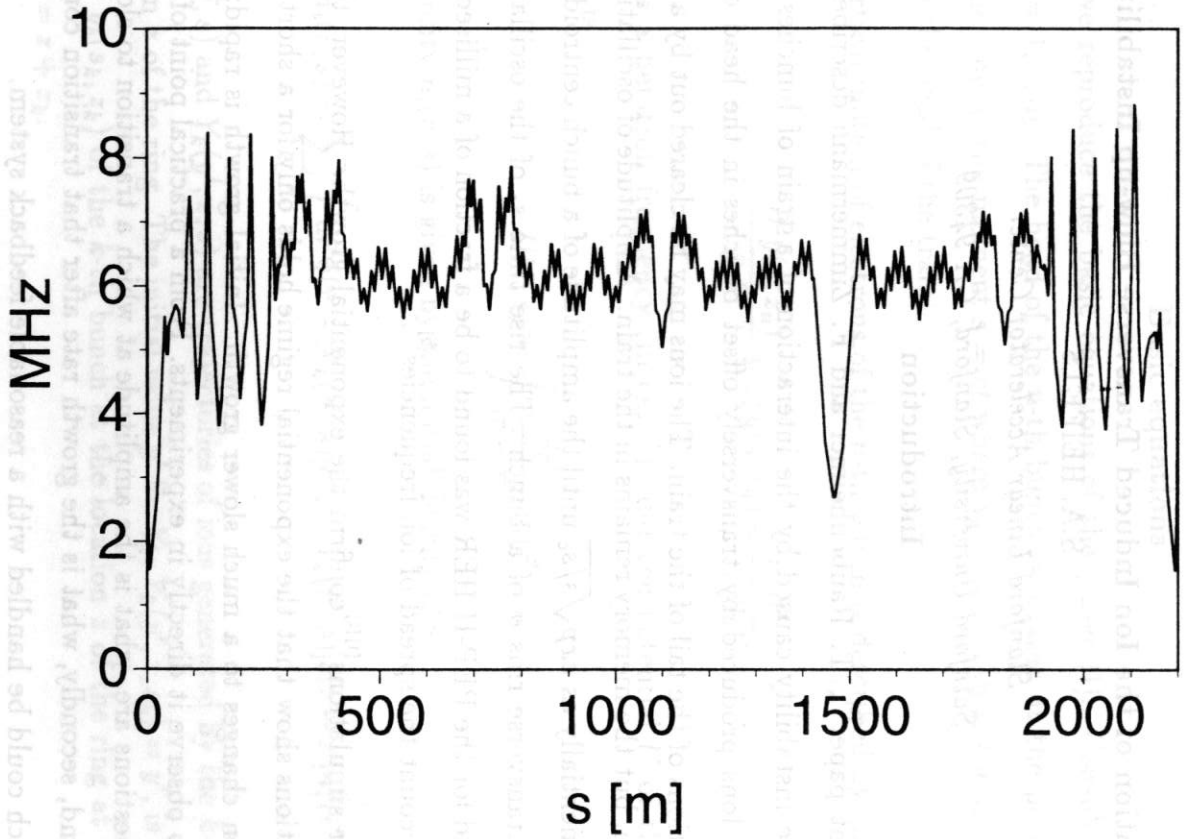

Fig. 9.